Contrib Mineral Petrol (2007) 154:371–383
DOI 10.1007/s00410-007-0198-4

ORIGINAL PAPER

High-pressure partial melting of gabbro and its role in the Hawaiian magma source

G. M. Yaxley · A. V. Sobolev

Received: 13 August 2006 / Accepted: 23 March 2007 / Published online: 11 April 2007

Abstract We have conducted high-pressure experiments on a natural oceanic gabbro composition (Gb108). Our aim was to test recent proposals that Sr-enrichment in rare primitive melt inclusions from Mauna Loa, Hawaii, may have resulted from melting of garnet pyroxenite formed in the magma source regions by reaction of peridotite with siliceous, Sr-enriched partial melts of eclogite of gabbroic composition. Gb108 is a natural, Sr-enriched olivine gabbro, which has a strong positive Sr anomaly superimposed on an overall depleted incompatible trace element pattern, reflecting its origin as a plagioclase-rich cumulate. At high pressures it crystallises as a coesite eclogite assemblage, with the solidus between 1,300 and 1,350°C at 3.5 GPa and 1,450 and 1,500°C at 4.5 GPa. Clinopyroxenes contain 4–9% Ca-eskolaite component, which varies systematically with pressure and temperature. Garnets are almandine and grossular-rich. Low degree partial melts are highly siliceous in composition, resembling dacites. Coesite is eliminated between 50 and 100°C above the solidus. The whole-rock Sr-enrichment is primarily hosted by clinopyroxene. This phase dominates the mode (>75 wt%) at all investigated PT conditions, and is the major contributor to partial melts of this eclogite composition. Hence the partial melts have trace element patterns sub-parallel to those of clinopyroxene with ≈10× greater overall abundances and with strong positive Sr anomalies. Recent studies of primitive Hawaiian volcanics have suggested the incorporation into their source regions of eclogite, formerly gabbroic material recycled through the mantle at subduction zones. The models suggest that formerly gabbroic material, present as eclogite in the Hawaiian plume, partially melted earlier than surrounding peridotite (i.e. at higher pressure) because of the lower solidus temperature of eclogite compared with peridotite. This produced highly siliceous melts which reacted with surrounding peridotite producing hybrid pyroxene + garnet lithologies. The Sr-enriched nature of the formerly plagioclase-rich gabbro was present in the siliceous partial melts, as demonstrated by these experiments, and was transferred to the reactive pyroxenite. These in turn partially melted, producing Sr-enriched picritic liquids which mixed with normal picritic partial melts of peridotite before eruption. On rare occasions these mixed, relatively Sr-rich melts were trapped as melt inclusions in primitive olivine phenocrysts.

Keywords Eclogite · Gabbro · Hawaiian picrite · Mantle melting

Communicated by: J. Hoefs.

Electronic supplementary material The online version of this article (doi:10.1007/s00410-007-0198-4) contains supplementary material, which is available to authorized users.

G. M. Yaxley (✉)
Research School of Earth Sciences,
The Australian National University,
Mills Road, Canberra, ACT 0200, Australia
e-mail: Greg.Yaxley@anu.edu.au

A. V. Sobolev
Vernadsky Institute of Geochemistry,
Russian Academy of Sciences, Moscow, Russia
e-mail: sobolev@geokhi.ru

A. V. Sobolev
Max-Planck Institut für Chemie,
Abteiling Geochemie, Mainz, Germany
e-mail: asobolev@mpch-mainz.mpg.de

Introduction

Recent geochemical studies have emphasised the likely importance of the presence of multiple components in upper mantle magma source regions in the Hawaiian plume. Specific components additional to ambient peridotitic mantle, postulated on the basis of major and trace element, and stable and radiogenic isotopic (O, Hf, Os) evidence have included recycled oceanic basalt (Eiler et al. 1996; Lassiter and Hauri 1998), pelagic sediments (Blichert-Toft et al. 1999; Hauri 1996) and oceanic gabbro (Hofmann and Jochum 1996; Huang et al. 2005; Sobolev et al. 2000).

Unusually Sr-enriched melt inclusions trapped in primitive olivine phenocrysts from Mauna Loa picrites (Sobolev et al. 2000) were interpreted as evidence for the presence in their upper mantle sources, of discrete bodies of Sr-enriched gabbro, inferred to be recycled, formerly plagioclase-rich oceanic crustal cumulates. Such mafic lithologies would have crystallised as discrete bodies of eclogite at high pressure, which partially melted during adiabatic ascent in the peridotite-dominated Hawaiian plume, producing highly siliceous and Sr-rich liquids. These liquids infiltrated surrounding peridotite and interacted with it, producing hybrid pyroxene + garnet-rich lithologies (Yaxley and Green 1998) which inherited the Sr-rich (and presumably other trace element and isotopic) characteristics of the siliceous partial melts of eclogite (gabbro). Subsequent partial melting during adiabatic ascent of this hybrid material in the plume produced Sr-enriched, plagioclase-undersaturated picrites [the ghost plagioclase signature of Sobolev et al. (2000)], which mixed with much larger volumes of picrites produced by melting of normal peridotite, or peridotite similarly refertilised by other recycled components, prior to eruption. Early formed olivine phenocrysts in these magmas rarely trapped microsamples of the Sr-enriched component before mixing was complete.

Huang et al. (2005) have also recently postulated the presence of (formerly) plagioclase-rich gabbro in the source of lavas from the island of Kahoolawe, southwest of Maui in Hawaii, based on their higher $^{87}Sr/^{86}Sr$ at given $^{143}Nd/^{144}Nd$ compared with other Hawaiian shield volcanics. Similarly, ghost plagioclase signatures in melt inclusions in olivine were reported for Afar flood basalts (Kent et al. 2002) and Koulau lavas (Ren et al. 2005).

In order to test the possible involvement of gabbroic material in the Hawaiian mantle source, we have undertaken a high-pressure experimental study of the partial melting of an olivine gabbro composition at 3.5–4.5 GPa. In a second paper (Yaxley and Sobolev 2007), we report an investigation of interactions between partial melts of the gabbro and peridotite using layered experiments similar to those described by Yaxley and Green (1998). In particular, we seek to establish if recycled gabbroic material in the Hawaiian source could ultimately contribute to production of Sr-enriched picritic liquids such as those observed to have been incorporated into picritic melts trapped as inclusions in primitive olivine phenocrysts from some Mauna Loa lavas (Sobolev et al. 2000).

Experiments

Choice and preparation of starting composition

The composition chosen for the experiments was that of a natural olivine gabbro sample from DSDP Hole 753B, Leg 176 (SW Indian Ridge, near the Atlantis Fracture Zone at 57°E; depth 1,143.4 mbsf) (Snow 2002) which is henceforth referred to as Gb108 (Table 1). The sample is an olivine + plagioclase + clinopyroxene cumulate and was chosen because of the presence of a distinctive, positive Sr anomaly superimposed on an overall depleted whole-rock incompatible trace element pattern (Fig. 1). Such a Sr-rich gabbroic composition has been suggested as a suitable source material for the Sr-enriched component detected in rare olivine-hosted melt inclusions from Mauna Loa picrites (Sobolev et al. 2000). Major and trace element abundances for Gb108 are presented in Tables 1 and 2. Gb108 has CaO/Al_2O_3 of 0.74 and is low in FeO (5.96 wt%). Mg# (Mg# = 100 × Mg/[Mg + Fe*] where Fe* is total Fe calculated as Fe^{2+}) is 72.8.

There have been several recent experimental investigations of the partial melting of a range of mafic compositions at high pressures (Johnston 1986; Klemme et al. 2002; Pertermann and Hirschmann 2003a; Takahashi and Nakajima 2002; Takahashi et al. 1998; Yasuda et al. 1994; Yaxley and Green 1998). Gb108 is higher in SiO_2, Al_2O_3, MgO and CaO, and significantly lower in FeO and TiO_2 than most other studied compositions (Table 1). Na_2O and K_2O contents of Gb108 fall within the ranges of the other compositions. These distinctive features, and the overall Sr-enrichment, partly reflect the plagioclase-rich nature of Gb108.

The gabbro Gb108 was crushed and ground to a fine powder. This material was then fused in an Ar atmosphere in a box furnace at 1,300°C and quenched in water to produce a light green coloured glass. A portion of this glass was ground to a fine powder under analytical grade acetone using an agate mortar and pestle. The resultant powder was thoroughly dried at 200°C overnight and thereafter stored at 110°C to ensure it remained anhydrous. This material was used in subsequent piston-cylinder experiments. Remaining portions of the glass were analysed for major and minor elements by electronprobe microanalysis (EPMA) and for trace elements by laser ablation ICP-MS (Tables 1, 2).

Table 1 Compositions of Gb108 and other mafic compositions used in recent similar high-pressure experimental investigations

	Gb108	GA1	G2	G2K	CRB72-31	CLG46	SBM6	NAM-7	SSS.1.4	77SL-582	MIX1G
SiO_2	52.04	50.35	50.05	50.81	50.76	40.77	52.00	49.71	50.48	46.38	45.56
TiO_2	0.42	1.49	1.97	1.90	1.48	1.11	4.50	1.71	0.62	0.63	0.90
Al_2O_3	16.68	16.53	15.76	15.22	16.02	15.15	18.50	15.68	17.55	16.42	15.19
FeO	5.96	9.83	9.35	9.03	9.52	12.55		9.36	8.31	7.64	7.77
MgO	8.93	7.94	7.90	7.91	8.23	8.07	8.80	8.43	7.06	16.48	16.67
CaO	12.36	9.60	11.74	11.68	10.77	9.59	11.00	11.73	11.47	10.74	11.48
Na_2O	3.26	3.49	3.04	3.02	2.29	2.74	4.00	2.76	2.00	0.99	1.44
K_2O	0.04	0.44	0.03	0.26	0.39	0.01	1.20	0.23	0.28	0.09	0.04
P_2O_5					0.14			0.02	0.15		
Total	99.69	99.67	99.84	99.83	99.60	89.99	100.00	99.63	97.92	99.59	99.05
CaO/Al_2O_3	0.74	0.58	0.74	0.77	0.67	0.63	0.59	0.75	0.65	0.65	0.76
Mg#	72.75	59.01	60.09	60.95	60.64	53.40	100.00	61.61	60.22	79.36	79.3

Gb108—Snow (2002); GA1—Yaxley and Green (1998); G2 and G2K—Pertermann and Hirschmann (2003a); CRB72-31—Takahashi et al. (1998); CLG46—Takahashi and Nakajima (2002); SBM6—Klemme et al. (2002); NAM-7—Yasuda et al. (1994); SSS.1.4—Johnston (1986); 77SL-582—Keshav et al. (2004); MIX1G—Kogiso et al. (2003)

$Mg\# = 100 \times Mg/(Mg + \sum Fe)$

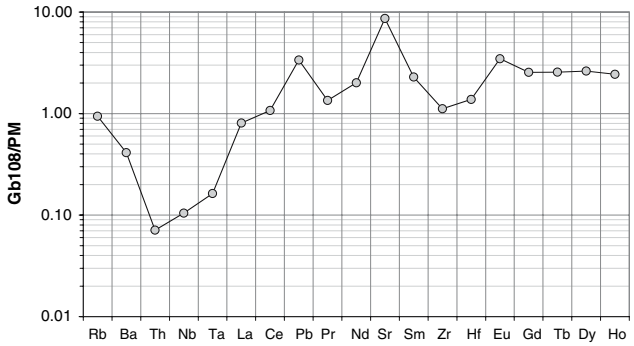

Fig. 1 Primitive mantle normalised trace element plot of Gb108. The data was obtained by LA-ICPMS of a glass made by quenching the fused Gb108 powder. Normalisation values are those of Sun and McDonough (1989)

Experimental and analytical techniques

All high-pressure experiments were conducted at The Australian National University. Experiments at 3.5 GPa were conducted in a conventional 1.27 cm piston-cylinder apparatus. Experiments at 4.5 GPa were run in an almost identical apparatus, with the exception that the WC piston and pusher surfaces were polished to a high quality optical finish using diamond paste. This procedure is believed to reduce surface cracks and imperfections, thus reducing potential stress points that could lead to fracture propagation under load.

The crushed Gb108 glass was encapsulated in graphite inner capsules, which were placed in Pt outer capsules, dried at 110°C for 2–3 h before sealing, and then sealed by arc welding in air immediately after removal from the drying oven.

Table 2 Trace element data for Gb108 glass

	Gb108 (ppm)
Cs	0.19
Rb	0.60
Ba	2.88
Th	0.01
U	0.10
Nb	0.08
Ta	0.01
La	0.56
Ce	1.90
Pb	0.62
Pr	0.37
Nd	2.73
Sr	183
Sm	1.02
Zr	12.5
Hf	0.43
Eu	0.58
Gd	1.52
Tb	0.28
Dy	1.94
Ho	0.40
Y	10.6
Er	1.14
Tm	0.16
Yb	1.10
Lu	0.16
Ni	51.6
Ti	2557

The high-pressure assemblies consisted of outer cylindrical NaCl-pyrex sleeves and an inner graphite tube furnace containing MgO spacers. The Pt capsule was surrounded by an alumina sleeve and thin alumina discs, preventing contact of the thermocouple bead with the capsule. All assembly components were stored at 110°C to prevent possible hydration.

For all experiments the sample assemblies were pressurised and brought to run temperature simultaneously. The hot-piston out technique was used, and pressure is accurate to ±0.01 GPa. Type B thermocouples (Pt_6Rh_{94}/$Pt_{30}Rh_{70}$) attached to Eurotherm 904 controllers were used to control temperature, which is accurate to ±10°C and precise to ±2°C. No correction was made for any effect of pressure on thermocouple output emf, and no friction correction was necessary because of use of NaCl sleeves. Experiments were quenched by terminating power to the furnace.

Capsules were recovered from the assemblies post-run, mounted in epoxy and sectioned longitudinally. The exposed run products were polished with diamond paste for examination and micro-beam analysis. Experimental conditions and phase assemblages produced are listed in Table 3.

Run products were examined using back-scattered electron images obtained on a JEOL 6400 Scanning Electron Microscope at the Electron Microscopy Unit, ANU. Crystalline phases were analysed in a JEOL JXA-8200 Superprobe at the Max-Planck Institut, Mainz, which was calibrated using natural USGS standards. Quantitative major and minor element analyses of the run products were obtained with an accelerating voltage of 15 kV and beam current of 20 nA using a finely focussed beam (1 μm) for analysis of crystalline phases. In order to minimise volatilisation of volatile elements (particularly alkalies) under the electron beam, experimentally quenched glass pools were analysed on the JEOL 6400 SEM, which had a LINK EDS detector fitted, using an accelerating voltage of 15 kV and beam current of 1 nA.

Trace elements abundances were measured at the Max-Planck Institut für Chemie in Mainz by LA-ICPMS on the Finnegan Element 2 ICP-MS fitted with a 213 nm laser in the case of the Gb108 glass used in the experiments, and by SIMS using the Cameca ims-3f ion microprobe in the case of the mineral phases and quenched melts in the experimental run products. For both techniques KL2-G and ML3B-G standards (Jochum et al. 2000) were used as reference materials. The laser or ion beam diameters were typically 20–30 μm.

Melting and phase relations of Gb108 were investigated at 3.5 and 4.5 GPa and from 1,300 to 1,525°C. Experimental conditions and the assemblages produced are presented in Table 3. Analytical results are presented in eTables 1–3.

Experimental results

Phase relations of gabbro Gb108

Melting experiments using the Gb108 glass produced well-crystallised assemblages of clinopyroxene ± garnet ± coesite ± quenched liquid. Assemblages for each experiment are reported in Table 3, and summarised on Fig. 2.

The runs at 3.5 GPa and 1,300°C (D-306), and 4.5 GPa and 1,450°C (C-1907) were sub-solidus, crystallising as clinopyroxene + garnet + coesite, with no clearly detectable evidence of quenched liquid. Garnet crystals were euhedral and typically up to 15 μm across. Most garnet crystals contained multiple small, rounded inclusions of coesite, which was also frequently observed as anhedral grains interstitial to more abundant clinopyroxene and garnet. Clinopyroxene crystallised as subhedral to euhedral tabular grains, typically up to 10 μm long (Fig. 3a).

Table 3 Summary of nominal pressure and temperature of each experimental run using Gb108 and the assemblage produced. Temperatures calculated using the garnet-clinopyroxene geothermometer of Ellis and Green (1979), Labelled [E&G] are also presented

Run No.	Pressure (GPa)	Temperature		Duration (h)	Assemblage
		(°C)	[E&G] (°C)		
D-306	3.5	1,300	1,332	120	ga + cpx + co
C-1856	3.5	1,350	1,361	138	ga + cpx + co + L
C-1864	3.5	1,375	1,393	192	ga + cpx + co + L
C-1844	3.5	1,400	1,388	118	ga + cpx + L
C-1860	3.5	1,425		52	cpx + L
C-1907	4.5	1,450	1,436	29	ga + cpx + co
C-1891	4.5	1,475		91	ga + cpx + L
C-1908	4.5	1,475	1,445	22	ga + cpx + co + L
C-1910	4.5	1,500	1,498	5	ga + cpx + L
C-1879	4.5	1,500		29	cpx + L
C-1913	4.5	1,525	1,533	6.5	ga + cpx + L

ga garnet, *cpx* clinopyroxene, *co* pure SiO2 phase inferred to be coesite, *L* quenched liquid

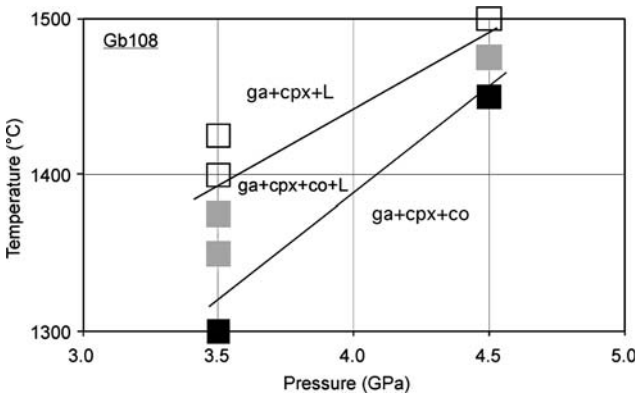

Fig. 2 Phase relations for Gb108 at 3.5 and 4.5 Pa. Abbreviations are as follows: *ga* garnet, *cpx* clinopyroxene, *co* coesite, *L* liquid. The *lower sloping line* is the approximate solidus; the *upper line* is the approximate position of coesite-out

The runs at 3.5 GPa and 1,350 and 1,375°C (C-1856 and C-1864) and at 4.5 GPa and 1,475°C (C-1908) produced clinopyroxene + garnet + coesite + quenched liquid. Grain-sizes were generally larger than sub-solidus runs, with garnets being up to 50 μm across and clinopyroxenes typically about 30 μm long. Glass occurred mainly at triple grain boundary junctions, in tiny (≤ 5 μm), non-interconnected pools in contact with crystal facets on the surrounding residual solid phases (Fig. 3b). Glassy pools sometimes contained tiny microlites, which were too small for analysis by electronprobe. Sometimes residual clinopyroxene crystals in contact with glassy pools exhibited thin rims (<1 μm) in contact with the glass, which were brighter than the rest of the crystal on back-scattered electron images. These microlites and rims are probably metastable clinopyroxene crystallised from glass during quenching. Similar quench-related garnet rims were not observed on residual garnet grains.

With increasing temperature, coesite was eliminated between 1,375 and 1,400°C at 3.5 GPa and between 1,475 and 1,500°C at 4.5 GPa, resulting in assemblages of clinopyroxene + garnet + quenched liquid in runs C-1844 and C-1910. In both these runs, the degree of melting was clearly greater than in the lower T runs described earlier. C-1910 contained approximately triangular pools of quenched melt greater than 5 μm across at triple grain boundary junctions, as well as thin films along double grain boundaries (Fig. 3c). Melt in this run was probably not quite interconnected throughout the charge. By 1,525°C at 4.5 GPa (C-1913) quenched melt in equilibrium with garnet + clinopyroxene appeared fully interconnected throughout the observable part of the sample.

The run at 3.5 GPa and 1,400°C (C-1844) contained a higher, fully interconnected quenched melt fraction and euhedral crystals of clinopyroxene (Fig. 3d).

In C-1910 minor evidence of quench-related crystallisation of metastable clinopyroxene as microlites within the pools and rims on residual clinopyroxene was again observed. The effect is more significant than in lower temperature runs, with most residual clinopyroxene crystals in contact with melt pools exhibiting thin bright rims on back-scattered electron images. These effects appear to be largely absent from C-1844.

At 3.5 GPa, garnet was eliminated by 1,425°C, resulting in an assemblage of clinopyroxene + quenched liquid

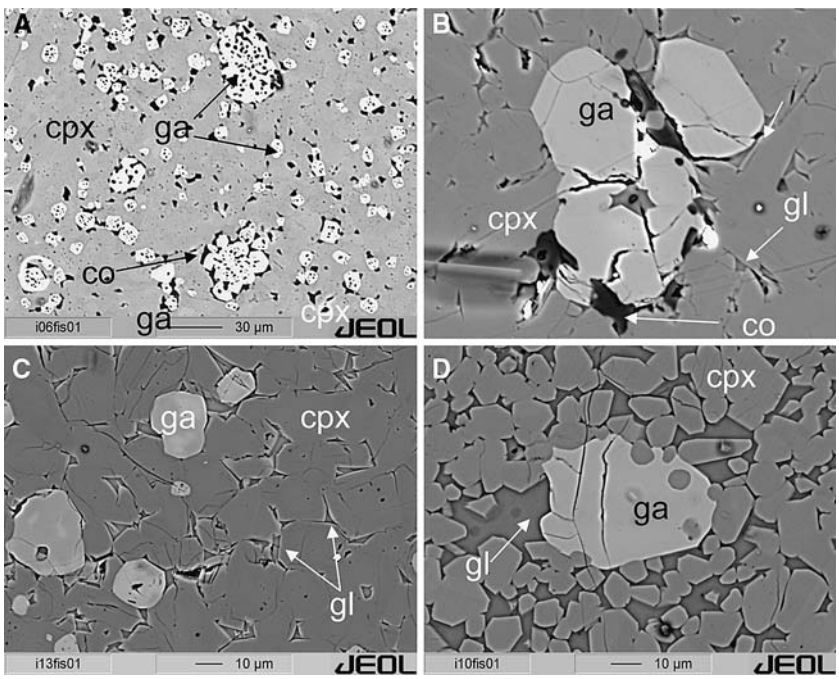

Fig. 3 Back-scattered images of experimental runs. **a** D-306 at 3.5 GPa and 1,300°C, showing sub-solidus assemblage of co + ga + cpx. **b** C-1908 at 4.5 GPa and 1,475°C showing assemblage of co + ga + cpx + quenched liquid (*gl*). **c** C-1910 at 4.5 GPa and 1,500°C showing assemblage of ga + cpx + gl, and **d** C-1844 at 3.5 GPa and 1,400°C, showing assemblage of ga + cpx + gl. Scale for **b** is the same as **c** and **d**

(C-1860). At 4.5 GPa, garnet persisted at least to 1,525°C (C-1913).

Two additional 4.5 GPa runs (C-1891 at 1,475°C and C-1879 at 1,500°C) produced assemblages of garnet + clinopyroxene + liquid and clinopyroxene + liquid respectively. In the case of C-1879 this assemblage was unexpected, given that C-1913 at 1,525°C contained garnet + clinopyroxene + liquid. C-1891 and C-1879 exhibited evidence of melt segregation and migration, with melt unevenly distributed in the experimental sample, often forming large pools containing glass and metastable quench phases. Residual phase compositions were variable in different parts of these assemblages and inconsistent with temperature-based trends exhibited by other runs. We believe these effects may have been caused by strong temperature gradients in the encapsulated material (possibly due to heater deformation or shearing), and we exclude data from these experiments from following discussions of the major and minor element systematics. However, the formation of large quenched melt pools did allow precise SIMS determination of trace elements, and this data is considered in a later section.

Garnet compositions

Garnets compositions are presented in eTable 1. They contain 50.0–55.2 mol% pyrope, 18.2–22.2 mol% grossular and 23.3–28.6 mol% almandine. At 3.5 GPa garnet Mg# [where Mg# = 100 × Mg/(Mg + ∑Fe)] increases systematically from 63.9 just below the solidus to 67.6 at 1,400°C. At 4.5 GPa garnet Mg# increases from 64.2 just above the solidus (1,450°C) to 70.4 at 1,525°C, consistent with increasing degrees of partial melting with increasing temperature.

Clinopyroxene compositions

Most compositional parameters of the clinopyroxenes (eTable 2) vary systematically with increasing temperature at each pressure. For example, clinopyroxene TiO_2 generally decreases with increasing temperature at both pressures. Na_2O content decreases systematically with temperature in the 3.5 GPa runs, but remains fairly constant over the range of temperatures of the 4.5 GPa runs (except for C-1910 where it is unexpectedly higher than in other 4.5 GPa runs). At 3.5 GPa, Mg# initially decreases from 77.3 to 74.5 from 1,300 to 1,375°C (sub-solidus to above solidus) but then increased to 79.0 with increasing temperature. A similar pattern was observed in the 4.5 GPa runs, with clinopyroxene Mg# initially decreasing from 76.3 to 75.2 from sub-solidus to the lowest temperature above solidus run, and then increasing with temperature to 78.0 at 1,525°C.

Clinopyroxene Al_2O_3 contents are very high (16.3–17.5 wt%), considerably higher than those reported by Pertermann and Hirschmann (2003a) (11.0–15.7 wt%), Klemme et al. (2002) (14–16 wt%) or Yaxley and Green (1998) (13.8–14.9 wt%), presumably partly reflecting the high bulk Al_2O_3 content of Gb108 compared with other studied materials (Table 1).

We calculated structural formulae of the clinopyroxenes assuming all Fe was present as Fe^{2+} (eTable 2). Cation totals (assuming six O-atoms per unit cell) were consistently below 4.000, ranging from 3.898 to 3.957. Assuming that Fe^{3+} is negligible (likely under the fO_2 conditions of these experiments, which were probably buffered at or near CCO), this suggests that the clinopyroxenes are cation deficient. The pyroxenes contain excess Al on the octahedral site (Al^{VI}), i.e. Al that cannot be accommodated in jadeite or Ca-Tschermak's components (Hermann 2003). A strong negative correlation between cation total and excess Al^{VI} indicates that the cation deficiency is due to the presence of significant Ca-eskolaite ($Ca_{0.5}[\bullet]_{0.5}AlSi_2O_6$) in these experimental pyroxenes, as was also reported for natural high pressure pyroxenes (Sobolev and Sobolev 1977) and for clinopyroxene crystallised during similar experimental studies by Pertermann and Hirschmann (2003a) and Klemme et al. (2002).

The components jadeite ($NaAlSi_2O_6$), diopside ($CaMgSi_2O_6$), enstatite–ferrosilite ($Mg_2Si_2O_6$–$Fe_2Si_2O_6$), Ca-Tschermaks ($CaAl_2SiO_6$), Al-buffonite ($CaMg_{0.5}Ti_{0.5}AlSiO_6$) and Ca-eskolaite ($Ca_{0.5}[\bullet]_{0.5}AlSi_2O_6$) were calculated following the method described by Pertermann and Hirschmann (2003a) (eTable 2). They contain 8.2–19.2 mol% Ca-eskolaite, corresponding to ≈4–9% of the M2-sites in these crystals being vacant.

In Fig. 4, the amount of Ca-eskolaite per formula unit is plotted against run temperature for the 3.5 and 4.5 GPa runs. Ca-eskolaite increases with increasing temperature at both pressures for runs that contain free crystalline SiO_2 in the assemblage (inferred to be coesite). In runs from which coesite was eliminated due to partial melting, Ca-eskolaite component decreases with increasing temperature at both pressures. This is consistent with formation of the Ca-eskolaite component by the following reaction, representing solid solution of excess silica and clinopyroxene

$$\underset{\text{Ca-Eskolaiteincpx}}{Ca_{0.5}[\bullet]_{0.5}AlSi_2O_6} = 0.5\ \underset{\text{Ca-Tschermak's}}{CaAl_2SiO_6} + \underset{\text{Silicainmeltorcoesite}}{1.5\ SiO_2}$$

The negatively sloped segments of the trends on Fig. 4 reflect decreasing silica activity (a_{SiO_2}) with increasing temperature from below coesite-out (a_{SiO_2} buffered by coesite) to above coesite-out (a_{SiO_2} buffered by siliceous liquid). At $T >$ co-out a_{SiO_2} decreases with increasing

temperature as other components are progressively added to the melt, driving the reaction to the right and resulting in progressively lower Ca-eskolaite in cpx. The higher pressure (and temperature) coesite-bearing runs have slightly higher Ca-eskolaite component in their clinopyroxenes, consistent with overall greater solid solution between excess silica and clinopyroxene at high pressure and/or temperature.

The clinopyroxenes contain 19.4–26.6 mol% jadeite. In 3.5 GPa runs, jadeite decreases systematically with increasing temperature (% melting). However, at 4.5 GPa the variation is non-systematic and small (21.0–23.7 mol%), reflecting a change in Na behaviour from incompatible at 3.5 GPa to nearly compatible at 4.5 GPa.

Partial melt compositions

We were unable to determine melt compositions from runs C-1856 and C-1864 (3.5 GPa and 1,350 and 1,375°C, respectively) due to the small size of the melt pools (<2 μm). In order to minimise volatilisation of alkali components, quenched liquid pools in other runs (eTable 3) were determined using a 1 nA beam current on a JEOL 6400 SEM fitted with a Link EDS detector. Where possible a broad electron beam was used in an attempt to include both metastable quench phases and glass in the analysed area, thus minimizing the effect of quench-related compositional modification of equilibrium liquids. However, in C-1908, where melt pools were small (generally <5 μm across) a focussed 1 μm 1 nA beam was necessary. Despite these precautions, the compositions in eTable 3 have not yet been tested using the layered or sandwich experimental technique (Falloon and Green 1987).

The estimated melts are broadly dacitic at low degrees of melting, consistent with previous high pressure partial melting studies of coesite-bearing eclogitic compositions (e.g. Yaxley and Green 1998). For example, the lowest temperature melt-bearing run at 4.5 GPa (C-1908) contains 64.4 wt% SiO_2. Liquid SiO_2 contents decrease systematically with increasing temperature at both pressures such that the highest degree partial melts are broadly andesitic. Abundances of MgO, FeO and CaO are low. Al_2O_3 contents are high, varying from 15.4 to 18.2 wt%, with a tendency to be higher in the lower pressure runs. K_2O and TiO_2 in melts decrease systematically with increasing temperature at both pressures reflecting their incompatible nature during partial melting of garnet and clinopyroxene. Na_2O decreases with increasing temperature in the 3.5 GPa runs but is approximately constant over a range of temperatures in the 4.5 GPa runs, suggesting compatible behaviour.

The accuracy of the measured compositions was tested using mass balance calculations. For each experiment, a least squares multiple regression was applied to the data according to the equation

$$C_i^{\mathrm{Gb108}} = F^{\mathrm{cpx}} \times C_i^{\mathrm{cpx}} + F^{\mathrm{ga}} \times C_i^{\mathrm{ga}} + F^{\mathrm{co}} \times C_i^{\mathrm{co}} + F^{\mathrm{liq}} \times C_i^{\mathrm{liq}}$$

where C_i^{phase} is the concentration of component i in each phase present in the experiment or in Gb108, and F^{phase} is the mass fraction of that phase (*cpx* = clinopyroxene, *ga* = garnet, *co* = coesite, *liq* = quenched liquid). The results are presented in Table 4. Calculations for all experiments produced satisfactory mass balances with the exception of C-1908, which produced a small negative liquid fraction. Analysis of the quenched liquid in C-1908 using a 1 μm electron-beam rather than the broad beam scans employed for other experiments, may have been compromised by metastable quench-related phases in the analysed melt pools and on the rims of equilibrium crystals in contact with the melt pools. We therefore conclude that this measured composition is not accurate and do not consider it further.

Approach to equilibrium

We used the temperature dependence of exchange of Fe^{2+} and Mg between garnet and clinopyroxene, calibrated by Ellis and Green (1979), to assess the extent of equilibration of garnet and clinopyroxene that crystallised in the current experiments. Assuming that Fe was present in both phases only as Fe^{2+}, and with the exception of C-1864, all calculated temperatures (Table 3) are within 35°C of the nominal experimental temperature, and in many cases are within 20°C, within the quoted uncertainty of the thermometer of ±5% (Ellis and Green 1979) (excluding C-1891 and C-1979 in which evidence for strong thermal

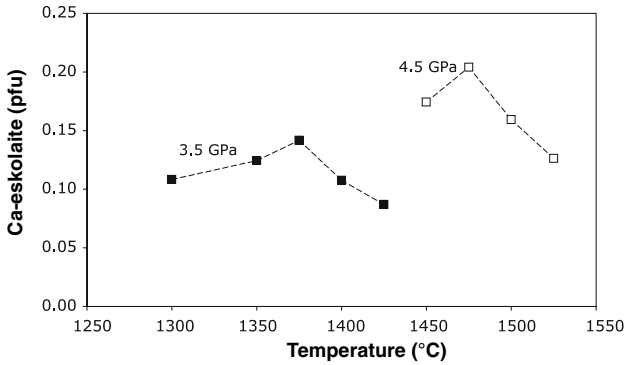

Fig. 4 Plot of Ca-eskolaite component (per formula unit) for the experimental clinopyroxenes, calculated following Pertermann and Hirschmann (2003a)

gradients was observed). Garnet and clinopyroxene from C-1864 returned a calculated temperature 71°C higher than the nominal temperature of 1,375°C, a 5.2% discrepancy. The very good general agreement between nominal and calculated run temperatures, along with the homogeneity of measured phase compositions in each run, indicates a very close approach to chemical equilibrium in these runs.

Phase and liquid trace element compositions

Trace element abundances of garnet, clinopyroxene and quenched liquids in 4.5 GPa experiments C-1879, C-1891, C-1907, C-1910 and C-1913 were measured by SIMS. Data is presented in eTable 4 with representative normalised trace element plots in Fig. 5.

Garnets were typically strongly enriched in Heavy Rare Earth Elements (HREE), and exhibited the usual strong fractionation of HREE from Light REE (LREE). Primitive mantle normalised Ce/Yb ($[Ce/Yb]_{pm}$) values for garnets were 0.04 for the sub-solidus run C-1907 and run C-1910 with 11.3% liquid, but decreased substantially to 0.007 for run C-1913 which contained 17.6% liquid. HREE abundances did not vary significantly with degree of melting. Garnet grains also exhibited negative Ti anomalies.

Clinopyroxenes exhibit convex downward REE patterns, peaking at Eu. Primitive mantle normalised La abundances varied from 0.90 to 0.10 with increasing temperature. HREE abundances were similar however, with PM-normalised Yb values of 1.0–1.1 over the temperature range. The most striking feature of the clinopyroxene trace element patterns is the strong positive Sr and Eu anomalies and slight negative Zr anomalies.

Quenched liquid's trace element patterns are sub-parallel to the clinopyroxene patterns at about 10× higher abundances. They are characterised by fairly flat mantle normalised patterns for the moderately incompatible trace elements, including the MREE and HREE. Highly incompatible elements such as Nb and K are depleted. Again, the most distinctive feature of the liquids' trace element patterns is the strong positive Sr anomaly observed in quenched liquids in both 4.5 GPa super-solidus runs.

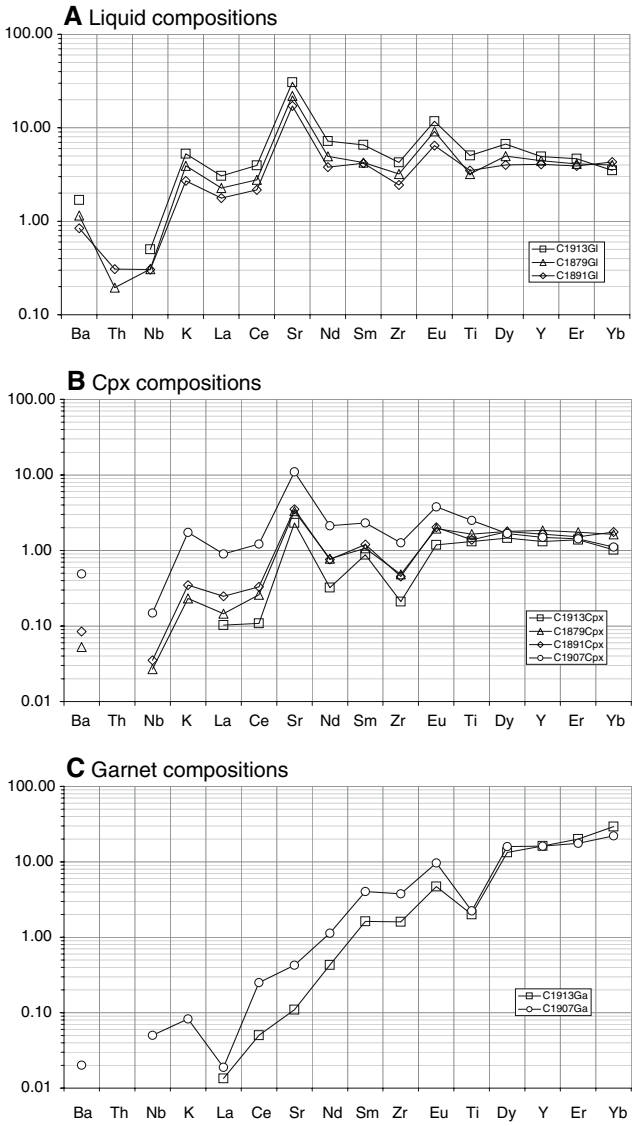

Fig. 5 Primitive mantle normalised plots of SIMS trace element analyses of glasses, clinopyroxenes and garnets from the Gb108 experiments

Clinopyroxene/liquid partition co-efficients (D^{cpx}) calculated from data obtained from the 4.5 GPa experiments are presented in Fig. 6a, where they are also compared with

Table 4 Abundances as mass fractions (F) of phases and quenched liquids in Gb108 runs, calculated from least squares fitting of phase and estimated liquid compositions

	D-306 ga + cpx + co	C-1844 ga + cpx + L	C-1860 cpx + L	C-1907 ga + cpx + co	C-1908 ga + cpx + co + L	C-1910 ga + cpx + L	C-1913 ga + cpx + L
F[ga]	0.145 (0.014)	0.029 (0.015)	0.000 (0.000)	0.085 (0.000)	0.047 (0.022)	0.067 (0.022)	0.022 (0.019)
F[cpx]	0.795 (0.017)	0.777 (0.026)	0.721 (0.024)	0.859 (0.023)	0.927 (0.038)	0.834 (0.044)	0.759 (0.042)
F[co]	0.052 (0.005)	0.000 (0.000)	0.000 (0.000)	0.040 (0.032)	0.019 (0.015)	0.000 (0.000)	0.000 (0.000)
F[liq]	0.000 (0.000)	0.185 (0.018)	0.264 (0.020)	0.000 (0.009)	-0.005 (0.042)	0.092 (0.030)	0.210 (0.033)

Numbers in parentheses are standard errors

the values presented by Pertermann and Hirschmann (2002). Except for the most highly incompatible elements, our data agree extremely well with this data. D^{cpx} determined from C-1891 and C-1879 for K, La, Ce, and to a lesser extent Sr, are significantly to slightly higher than the values reported by Pertermann and Hirschmann (2002), possibly reflecting minor overlap of the ion beam on adjacent glass when analysing relatively small clinopyroxene crystals. For other less incompatible or compatible trace elements, this apparently has an insignificant effect due to the lower relative abundances of these elements in the glass. When plotted on an Onuma diagram (Fig. 7; D^{cpx} vs. effective ionic radius) a well-constrained curve is evident. This data can be fitted to an equation describing the lattice strain model for trace element partitioning (Blundy and Wood 2003), and the resultant curve is plotted on Fig. 7.

Garnet/liquid partition coefficients (D^{ga}) are presented in Fig. 6b, and compared with those reported by Pertermann et al. (2004) for garnets crystallised from a MORB-like composition at 2.9–3.1 GPa. In general, our data are within the range of Pertermann's data, with the exception of some of the most incompatible elements (K and La) in C-1910. The apparent constancy of D^{ga}s measured in C-1910 for the most incompatible elements (K, La, Ce, Pr and Sr) suggests again that minor beam overlap onto adjacent glass may have been a problem during SIMS analysis of the garnet crystals in this run product.

Discussion

Mineral and melting modes

In line with recent similar studies (Pertermann and Hirschmann 2003a, b), sub-solidus runs using Gb108 (D-306 and C-1907) crystallised highly aluminous clinopyroxene with broadly similar overall compositions to the bulk composition (Tables 1 and eTable 2). Hence, clinopyroxene dominates the mode of Gb108 (75.9–85.9 wt%) in these high-pressure runs. However, in detail, the clinopyroxene has slightly higher Al_2O_3 and CaO, and slightly lower SiO_2 and FeO than Gb108 bulk, requiring for sub-solidus mass balance, co-crystallisation of small amounts of low-Al, Si-rich coesite and relatively FeO-rich garnet.

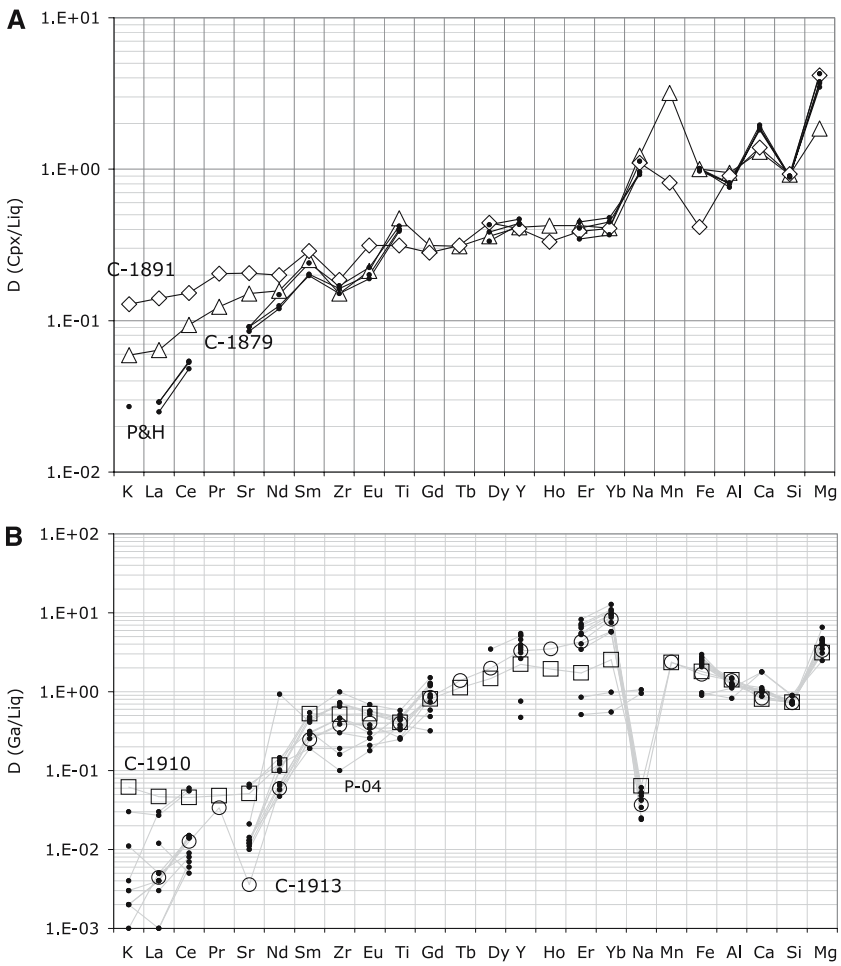

Fig. 6 Comparison of *D* values for trace element partitioning **a** between cpx and liquid (cpx/liquid) for the Gb108 experiments C-1891 and C-1879 (*large diamonds* and *triangles*) and those of Pertermann and Hirschmann (2002) (*small black circles*; P&H), and **b** between garnet and liquid (ga/liquid) for Gb108 experiments C-1910 and C-1913 and those of Pertermann et al. (2004) (*small black circles*; P-04)

A distinctive feature of the Gb108 composition is the relatively low modal abundance of garnet (and conversely relatively high modal abundance of clinopyroxene) compared with GA1 (Yaxley and Green 1998). For example, the garnet-bearing runs in the present study crystallised between 2.2 and 14.5 wt% garnet and 72.1–92.7 wt% clinopyroxene, compared with the experiments of (Yaxley and Green 1998) in which GA1 crystallised from 9.1 to 26.8 wt% garnet and 4.5–60.6 wt% clinopyroxene. This again is because Gb108 clinopyroxenes compositions are much closer to the Gb108 bulk composition than are the GA1 clinopyroxenes to GA1 bulk composition.

The variation in phase proportions with temperature for the Gb108 melting experiments is plotted in Fig. 8. Modes of all phases decrease with increasing temperature above the solidus, indicating that all three phases are contributing to the liquid during near-solidus eutectic-style melting. Given its modal dominance, clinopyroxene is the major contributing phase. However, at low degrees of melting coesite contributes until it is exhausted 50–100°C above the solidus. As noted by Pertermann and Hirschmann (2003a) garnet, although low in abundance, persists throughout the melting interval at least over the range of temperatures investigated.

Partial melt compositions

Recent discussion has focussed on whether or not low degree (quartz/coesite saturated), high pressure, anhydrous partial melts of mafic compositions are highly siliceous, i.e. dacitic versus andesitic. Yaxley and Green (1998) reported low degree (≈13%) partial melts of an average altered oceanic crustal composition (GA1) at 3.5 GPa, and 1,250 and 1,300°C with ≈63–65 wt% SiO_2, clearly dacitic. These liquids were in equilibrium with coesite eclogite residue. In contrast, Pertermann and Hirschmann (2003a) reported andesitic glasses with 55–57 wt% SiO_2 at a slightly lower pressure (3.0 GPa), in equilibrium with quartz eclogite. They attributed the difference to different starting compositions, in particular to the contrasting K_2O contents. GA1 has high K_2O (0.44 wt%) and therefore its low degree partial melts have as much as 3.8 wt% K_2O (Yaxley and Green 1998), whereas G2 contains only 0.03 wt% K_2O and produced low degree partial melts with 0.24–1.1 wt% K_2O. To illustrate this point, Pertermann and Hirschmann (2003a) also conducted partial melting experiments on a potassium-enhanced composition G2K with 0.26 wt% K_2O, and produced dacitic partial melts with 1.4–1.6 wt% K_2O and 61–64 wt% SiO_2.

The current results for Gb108 suggest that other factors apart from bulk K_2O-content influence the silica content of melts. Gb108 contains only 0.04 wt% K_2O but we have succeeded in producing highly siliceous dacitic partial melts (up to ≈61–64 wt% SiO_2) with far less K_2O than low degree partial melts of G2 (Pertermann and Hirschmann 2003a) (eTable 3). For example, C-1844 (3.5 GPa, 1,400°C) contained 18.5 wt% liquid with 62 wt% SiO_2 and 0.19 wt% K_2O. At 4.5 GPa, C-1910 contained 9.16 wt% liquid with 61.3 wt% SiO_2 and 0.36 wt% K_2O. We believe our melt compositions are reasonable estimates based on their generally systematic compositional variation with temperature and the reasonable fit of least squares mass balance calculations using bulk, liquid and phase compositional data (Table 4).

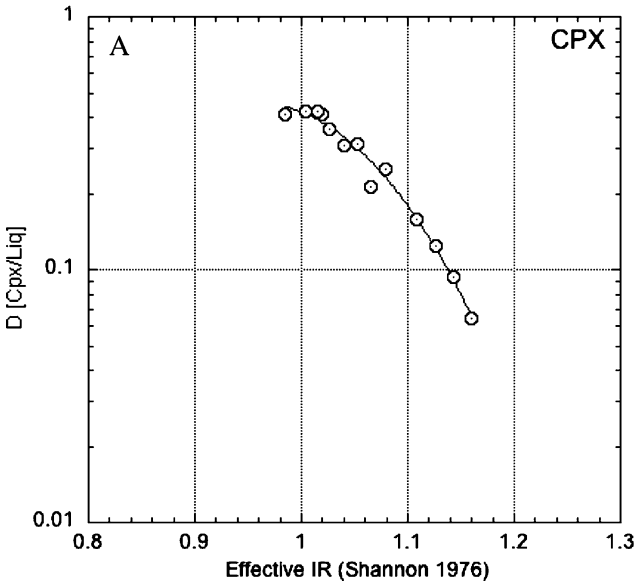

Fig. 7 Onuma diagram for trace element partitioning between clinopyroxene and liquid. *Solid line* is weighted multiple regression to the equation describing the lattice strain model for partitioning (Blundy and Wood 2003). Effective ionic radii (*IR*) are from (Shannon 1976)

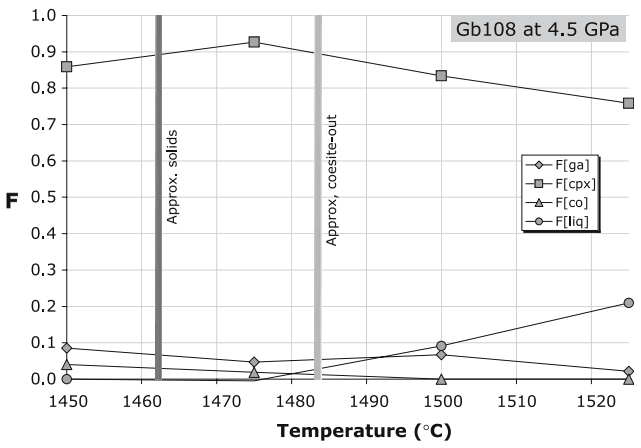

Fig. 8 Fractions by weight of crystalline phases and liquid in Gb108 melting runs at 4.5 GPa, calculated by least squares regression of bulk, phase and liquid compositions

Liquids saturated in coesite have their silica activity buffered by the coesite. As pointed out by Pertermann and Hirschmann (2003a), this means the SiO_2 concentration of the liquid can only be increased by components that decrease the activity coefficient of SiO_2, such as K_2O (Hirschmann et al. 1998; Ryerson 1985), as clearly demonstrated by Pertermann's comparison between quartz-saturated partial melts of bulk compositions G2 and G2K (which are identical except that G2K is significantly enhanced in K_2O content). However, our gabbroic composition Gb108 has also significantly lower TiO_2 than G2 (0.42 vs. 1.97 wt%) with similar K_2O content. As expected, coesite-saturated partial melts of Gb108 have lower TiO_2 contents (eTable 3) than those of G2 or G2K (Table 3 of Pertermann and Hirschmann 2003a), which are in many cases rutile-saturated. TiO_2 has the opposite effect on silica activity coefficients to K_2O (Pertermann and Hirschmann 2003a; Xirouchakis et al. 2001), and therefore the SiO_2 concentration in coesite-saturated partial melts of low K Gb108 may have been enhanced (despite their low K) by their relatively low TiO_2 concentrations, or SiO_2 in G2 partial melts may have been depressed by its high TiO_2 content.

''Live'' versus ''ghost'' plagioclase signatures

Recently, the relative Sr enrichment of incompatible element depleted melts (melt inclusions and matrix glasses) from mid-ocean ridges and Iceland were prescribed to interaction of mantle-derived melts with gabbroic crust (Danyushevsky et al. 2003; Gurenko and Sobolev 2006). This process by definition requires that resultant melts are saturated by plagioclase, which is the major mineral of gabbro. Thus a ''live'' plagioclase signature is developed by melts which gain excess Sr by reaction with actual plagioclase [see Sobolev et al. (2000); Gurenko and Sobolev (2006) for numerical modeling]. In contrast, all reported Hawaiian Sr-rich melts are severely plagioclase undersaturated according to their major element compositions (Ren et al. 2005; Sobolev et al. 2000) and thus do not indicate any reaction with plagioclase. However, these Hawaiian melts yield distinct trace element signatures of plagioclase (''ghost plagioclase''; Sobolev et al. 2000), which therefore calls for other processes than reaction with plagioclase bearing rocks.

Sr-enrichment in high pressure partial melts of gabbro and Hawaiian source modification

The presence of discrete gabbroic heterogeneities in the peridotite-dominated source regions of some Hawaiian lavas has been recently suggested, based on the discovery of unusually Sr-enriched melt inclusions hosted by primitive olivine in picrites erupted on Mauna Loa (Sobolev et al. 2000) and Koolau (Ren et al. 2005), and on major, trace and isotopic characteristics of lavas erupted by the Kahoolawe Volcano (Huang et al. 2005).

However, the way in which heterogeneous mantle such as that proposed for the Hawaiian source regions, actually melts is poorly understood. Yaxley and Green (1998) developed a model in which melting of heterogeneous mantle (peridotite + eclogite) was controlled by a thermal divide on the liquidus surface in the high pressure ''eclogite tetrahedron'', which separated nepheline-normative, picritic minimum partial melts of peridotite from lower temperature, quartz-normative, dacitic partial melts of eclogite (O'Hara and Yoder 1967). Dacitic melts which come into contact with peridotite must react out of existence to form new phases lying on the thermal divide, namely pyroxenes and garnet. The compositions of these phases will be broadly intermediate between those crystallising in peridotite and eclogite under the same PT conditions. Progressive extraction of melt from eclogite residue (e.g. during upwelling) and interaction with surrounding ultramafic wall rock will drive residual eclogite (pyroxenite) phases to more refractory compositions, and will progressively react with surrounding peridotite to produce olivine-free pyroxenite (Sobolev et al. 2005, 2007).

The extreme Sr-enrichment observed in clinopyroxene crystallised from Gb108, combined with that phase's high relative modal abundance, enhances the degree of Sr-enrichment in the partial melts, as the melts are dominated by components derived from clinopyroxene (Fig. 5). This Sr-enriched signature is likely to be passed onto ultramafic sources of some Hawaiian lavas in the manner described above and by Yaxley and Green (1998), as has been suggested by Sobolev et al. (2000). In the Hawaiian plume, we envisage discrete bodies of eclogitic material with gabbroic compositions, surrounded by ambient peridotite. The eclogitic material has Sr-enrichment due to former high modal plagioclase when the magma crystallised at low pressures, in the lower oceanic crust. However, at upper mantle pressures this enrichment is primarily hosted in clinopyroxene.

During adiabatic ascent in the plume the eclogite bodies will partially melt at greater depths than peridotite, due to the eclogite's lower solidus temperatures. The layered experiments of Yaxley and Green (1998) indicate that siliceous partial melts of eclogite will react out of existence with peridotite wall rock, replacing olivine with pyroxenes and garnet. In the case of Sr-enriched, siliceous partial melts of gabbro, the Sr-enrichment will be hosted mainly in newly crystallised pyroxenes. We have conducted a new series of layered experiments, in which Gb108 was run in a layered configuration with MORB-Pyrolite. These experi-

ments will be reported in detail in another paper (Yaxley and Sobolev 2007), but we observed complex interaction zones between the eclogitic and peridotite layers consisting of ortho- and clinopyroxene with minor garnet and olivine chemically isolated by newly grown orthopyroxene that we interpret as evidence of this process. Continued melting and redistribution of chemical components via a mechanism similar to that envisaged by Yaxley and Green (1998) could lead to formation of low degree picritic partial melts of pyroxenite (Sobolev et al. 2005), which would be strongly enriched in Sr. Subsequent mixing of these liquids with picritic partial melts of ambient peridotite could lead ultimately to formation of Sr-rich tholeiitic liquids similar to those trapped in primitive Mauna Loa (Sobolev et al. 2000) or Koolau (Ren et al. 2005) olivine phenocrysts, or erupted on Kahoolawe Volcano (Huang et al. 2005).

An alternative explanation of the anomalously Sr-rich melts observed by Sobolev et al. (2000) may related to the fact that D^{ga}[Sr] is approximately an order of magnitude lower than D^{ga}[Nd] in the current data set and in that of Pertermann et al. (2004) (Fig. 7b). Thus, a positive Sr-anomaly (i.e. high Sr/Nd) in the liquid may simply relate to the presence of garnet in the liquid's residue, and it may therefore be unnecessary to postulate recycled former gabbro with anomalous Sr in the Mauna Loa source to explain the observed anomalous Sr in the melt inclusions of Sobolev et al. (2000).

However, simple batch melting models suggest that this is unlikely to be the case. We define the magnitude of the Sr anomaly in terms of Sr_{PM}*, where Sr_{PM}* = Sr_{PM}/[(Pr_{PM} + Nd_{PM})/2] with abundances normalised to the Primitive Mantle values of Sun and McDonough (1989). If Sr_{PM}* = 1, there is no anomaly. If it is >1 a positive Sr anomaly exists relative to elements of similar incompatibility Pr and Nd. The liquids produced by partial melting of Gb108 in these experiments have Sr^*_{PM} from 3.3 to 3.7. Bulk Gb108 has Sr^*_{PM} = 5.2.

In Fig. 9 we use the Ds determined here to model simple batch melting of bimineralic eclogite (garnet + clinopyroxene) with 0–100% clinopyroxene. We use two source compositions, Gb108 (Table 2) and Gb108*. The latter is identical to Gb108 but with the Sr abundance artificially reduced from 183 to 35.4 ppm. This reduces the Sr_{PM}*, from 5.2 to 1.0, i.e. no Sr-anomaly. The models (Fig. 9) indicate that (a) Sr_{PM}* for partial melts of Gb108* for any mode do not deviate significantly from 1.0, and (b) partial melts of Gb108 for any mode vary only slightly from 5.2. We were unable to produce melts with Sr_{PM}* > 3 from Gb108* (with Sr_{PM}* = 1) regardless of the % melting, the proportions of garnet and clinopyroxene, or the experimentally measured Ds used [i.e. those of Pertermann and Hirschmann (2002) and Pertermann et al. (2004), or those calculated from our data in eTable 4]. Thus, unless the eclogitic source originally had a significant Sr-anomaly, it is very unlikely that partial melting in the presence of any proportions of garnet + clinopyroxene would produce a melt with a significant Sr-anomaly. We therefore conclude that the Sr anomaly measured in our experimental partial melts derives almost entirely from the high Sr_{PM}* of the gabbroic Gb108 source and not from the high D^{ga}[Sr]/D^{ga}[Nd] measured in the current dataset or in those of Pertermann and Hirschmann (2002) and Pertermann et al. (2004).

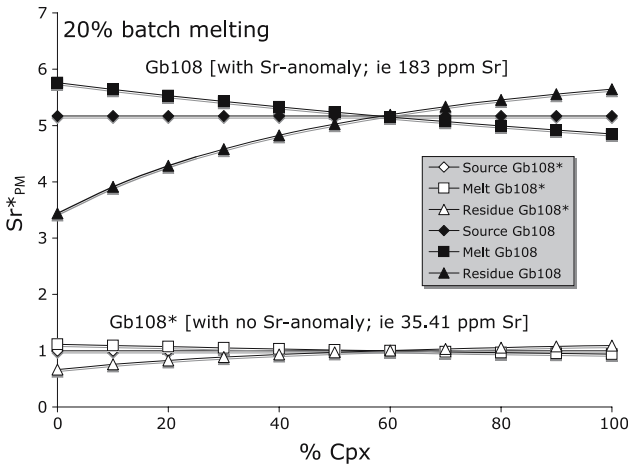

Fig. 9 Results of 20% batch melting models for garnet + clinopyroxene sources with percentage of clinopyroxene varied from 0 to 100% for sources Gb108 (Table 2) and Gb108* (Sr reduced from 183 to 35.41 ppm so that Sr_{PM}* = 1). Ds used are those from experiment C-1910, calculated from data presented in eTable 4. Similar results were obtained for other degrees of melting. See text for further information

Acknowledgments We gratefully acknowledge the assistance of Dean Scott and Bill Hibberson (high pressure laboratories, ANU), Frank Brink (Electron Microscopy Unit, ANU), Dmitry Kuzmin and Andrei Gurenko (Electron Microprobe Laboratory, MPI) and Kirstin Herwig (LA-ICPMS, MPI). Jon Snow kindly supplied the gabbro sample. An earlier version of this manuscript was materially improved after discussions with Carl Spandler. Constructive reviews from Marc Hirschmann and an anonymous reviewer are also much appreciated. The study was supported by Wolfgang Paul Award of the Alexander von Humboldt Foundation, Germany to A.V. Sobolev. Partial support from the following sources is also acknowledged: Russian Foundation of Basic Research RFBR grant 06-05-65234 and Russian President grant for leading Russian Scientific Schools НШ-4264.2006.5. both to A.V. Sobolev.

References

Blichert-Toft J, Frey FA, Albarede F (1999) Hf isotope evidence for pelagic sediments in the source of Hawaiian basalts. Science 285:879–882

Blundy J, Wood B (2003) Partitioning of trace elements between crystals and melts. Earth Planet Sci Lett 210:383–397

Danyushevsky LV, Perfit MR, Eggins SM, Falloon TJ (2003) Crustal origin for coupled 'ultra-depleted' and 'plagioclase' signatures in MORB olivine-hosted melt inclusions: evidence from the Siqueiros Transform Fault, East Pacific Rise. Contrib Mineral Petrol 144: 619–637

Eiler JM, Farley KA, Valley JW, Hofmann AW, Stolper EM (1996) Oxygen isotope constraints in the sources of Hawaiian volcanism. Earth Planet Sci Lett 144:453–468

Ellis DJ, Green DH (1979) An experimental study of the effect of Ca upon garnet-clinopyroxene Fe–Mg exchange equilibria. Contrib Mineral Petrol 71:13–22

Falloon T, Green D (1987) Anhydrous partial melting of MORB pyrolite and other peridotite compositions at 10 kbar: implications for the origin of primitive MORB glasses. Mineral Petrol 37:181–219

Gurenko AA, Sobolev AV (2006) Crust-primitive magma interaction beneath neovolcanic rift zone of Iceland recorded in gabbro xenoliths from Midfell, SW Iceland. Contrib Mineral Petrol 151:495–520

Hauri EK (1996) Major-element variability in the Hawaiian mantle plume. Nature 382:415–419

Hermann J (2003) Experimental evidence for diamond-facies metamorphism in the Dora-Maira massif. Lithos 70:163–182

Hirschmann MM, Baker MB, Stolper EM (1998) The effect of alkalis on the silica content of mantle-derived melts. Geochim Cosmochim Acta 62:883–902

Hofmann AW, Jochum KP (1996) Source characteristics derived from very incompatible trace elements in Mauna Loa and Mauna Kea basalts, Hawaiian Scientific Drilling Project. J Geophys Res 101:11831–11839

Huang S, Frey F, Blichert-Toft J, Fodor RV, Bauer GR, XU G (2005) Enriched components in the Hawaiian plume; Evidence from Kahoolawe Volcano, Hawaii. Geochem Geophys Geosyst 6

Johnston AD (1986) Anhydrous P–T phase relations of bear-primary high-alumina basalt from South Sandwich Islands. Contrib Mineral Petrol 92:368–382

Jochum KP, Dingwell DB, Rocholl A et al (2000) The preparation and preliminary characterisation of eight geological MPI-DING reference glasses for in-site microanalysis. Geostand Newslett 24:87–133

Kent AJR, Baker JA, Wiedenbeck M (2002) Contamination and melt aggregation processes in continental flood basalts: constraints from melt inclusions in Oligocene basalts from Yemen. Earth Planet Sci Lett 202:577–594

Keshav S, Gudfinnsson GH, Sen G, Fei Y (2004) High-pressure melting experiments on garnet clinopyroxenite and the alkalic to tholeiitic transition in ocean–island basalts. Earth Planet Sci Lett 223:365–379

Klemme S, Blundy JD, Wood BJ (2002) Experimental constraints on major and trace element partitioning during partial melting of eclogite. Geochim Cosmochim Acta 66:3109–3123

Kogiso T, Hirschmann MM, Frost DJ (2003) High-pressure partial melting of garnet pyroxenite: possible mafic lithologies in the source of ocean island basalts. Earth Planet Sci Lett 216:603–617

Lassiter JC, Hauri EH (1998) Osmium isotope variations in Hawaiian lavas: evidence for recycled oceanic lithosphere in the Hawaiian plume. Earth Planet Sci Lett 164:483–496

O'Hara MJ, Yoder HJ Jr (1967) Formation and fractionation of basic magmas at high pressures. Scott J Geol 3:67–117

Pertermann M, Hirschmann MM (2002) Trace element partitioning between vacancy-rich eclogitic clinopyroxene and silicate melt. Am Mineral 87:1365–1376

Pertermann M, Hirschmann MM (2003a) Anhydrous partial melting experiments on MORB-like eclogite: phase relations, phase compositions and mineral-melt partitioning of major elements at 2–3 GPa. J Petrol 44:2173–2201

Pertermann M, Hirschmann MM (2003b) Partial melting experiments on a MORB-like pyroxenite between 2 and 3 GPa: constraints on the presence of pyroxenite in basalt source regions from solidus location and melting rate. J Geophys Res 108:ECV12-11–ECV12-17

Pertermann M, Hirschmann MM, Hametner K, Günther D, Schmidt MW (2004) Experimental determination of trace element partitioning between garnet and silica-rich liquid during anhydrous partial melting of MORB-like eclogite. Geochem Geophys Geosyst 5:2003GC000638

Ryerson FJ (1985) Oxide solution mechanisms in silicate melts; systematic variations in the activity coefficients of silica. Geochim Cosmochim Acta 49:637–649

Ren ZY, Ingle S, Takahashi E, Hirano N, Hirata T (2005) The chemical structure of the Hawaiian mantle plume. Nature 436:837–840

Shannon RD (1976) Revised effective ionic radii and systematic studies of interatomic distances in halides and chalcogenides. Acta Crystallogr A32:751–767

Snow JE (2002) Major and trace element evolution of Hole 735B gabbros. In: Natland JH, Dick JH, Miller DJ, Von Herzen RP (eds) Proceedings of the ocean drilling program, scientific results, pp 1–18

Sobolev AV, Hofmann AW, Nikogosian IK (2000) Recycled oceanic crust observed in 'ghost plagioclase' within the source of Mauna Loa lavas. Nature 404:986–989

Sobolev AV, Hofmann AW, Sobolev SV, Nikogosian IK (2005) An olivine-free source of Hawaiian shield basalts. Nature 434:590–579

Sobolev AV, Hofmann AW, Kuzmin DV et al (2007) The amount of recycled crust in sources of mantle-derived melts. Science. doi:10.1126/Science.1138113

Sobolev VS, Sobolev AV (1977) Eclogite barrier at recrystallization of native basaltoids under conditions of high pressures. Dokl Akad Nauk 237:437–440

Sun S-s, McDonough WF (1989) Chemical and isotopic systematics of oceanic basalts: implications for mantle composition and processes. In: Saunders AD, Norry MJ (eds) Magmatism in the ocean basins. Geol Soc Spec. Publ. No. 42, pp 313–345

Takahashi E, Nakajima K (2002) Melting processes in the Hawaiian plume; an experimental study. In: Takahashi E, Lipman PW, Garcia MO, Naka J, Aramake S (eds) Hawaiian volcanoes; Deep underwater perspectives. Geophysical Monograph. American Geophysical Union, pp 403–418

Takahashi E, Nakajima K, Wright TL (1998) Origin of the Columbia River basalts: melting model of a heterogeneous plume head. Earth Planet Sci Lett 162:63–80

Xirouchakis D, Hirschmann MM, Simpson JA (2001) The effect of titanium on the silica content and on the mineral-liquid partitioning of mantle-equilibrated melts. Geochim Cosmochim Acta 65

Yasuda A, Fujii T, Kurita K (1994) Melting phase relations of an anhydrous mid-ocean ridge basalt from 3 to 20 GPa: implications for the behaviour of subducted oceanic crust in the mantle. J Geophys Res 99:9401–9414

Yaxley GM, Green DH (1998) Reactions between eclogite and peridotite: mantle refertilisation by subduction of oceanic crust. Schweiz Mineral Petrogr Mitt 78:243–255

Yaxley GM, Sobolev AV (2007) High pressure experimental investigation of interactions between partial melts of gabbro and peridotitic mantle (in press)

Contrib Mineral Petrol (2007) 154:371–383
DOI 10.1007/s00410-007-0198-4

High-pressure partial melting of gabbro and its role in the Hawaiian magma source

G. M. Yaxley & A. V. Sobolev

Electronic supplementary material

eTable 1: Garnet compositions from the Gb108 runs.

	D-306	C-1856	C-1864	C-1844	C-1907	C-1908	C-1910	C-1913
SiO_2	41.44	41.84	42.97	41.52	40.56	40.59	41.95	41.77
TiO_2	0.31	0.37	0.31	0.36	0.44	0.44	0.30	0.35
Al_2O_3	23.50	23.62	22.75	23.70	23.95	23.65	23.72	24.11
Cr_2O_3	0.02	0.01	0.01	0.01	0.01	0.01	0.02	0.02
FeO	13.92	14.13	13.45	13.19	13.49	13.85	12.03	11.67
MgO	13.80	14.44	14.25	15.41	13.97	13.93	14.88	15.54
MnO	0.37	0.37	0.34	0.36	0.35	0.34	0.33	0.33
NiO	0.02	0.00	0.00	0.01	0.01	0.01	0.02	0.02
CaO	7.85	7.09	7.51	7.14	8.64	8.12	8.11	8.17
Na_2O	0.11	0.04	0.05	0.05	0.06	0.07	0.09	0.06
K_2O	0.00	0.01	0.00	0.00	0.00	0.00	0.00	0.00
Total	101.33	101.93	101.64	101.76	101.49	101.02	101.45	102.04
Cations (12 O)								
Si	2.9959	3.0008	3.0778	2.9737	2.9344	2.9503	3.0031	2.9700
Ti	0.0169	0.0197	0.0169	0.0196	0.0239	0.0239	0.0162	0.0188
Al	2.0034	1.9973	1.9217	2.0016	2.0430	2.0268	2.0016	2.0213
Cr	0.0009	0.0007	0.0006	0.0008	0.0005	0.0008	0.0010	0.0012
Fe	0.8416	0.8473	0.8056	0.7902	0.8159	0.8417	0.7202	0.6941
Mg	1.4870	1.5439	1.5212	1.6457	1.5056	1.5088	1.5873	1.6472
Mn	0.0224	0.0224	0.0205	0.0216	0.0215	0.0212	0.0198	0.0197
Ca	0.6080	0.5450	0.5767	0.5484	0.6697	0.6326	0.6222	0.6223
Na	0.0151	0.0060	0.0065	0.0066	0.0089	0.0095	0.0132	0.0084
K	0.0004	0.0005	0.0000	0.0004	0.0002	0.0004	0.0003	0.0004
Ni	0.0010	0.0002	0.0000	0.0005	0.0008	0.0008	0.0013	0.0009
Total	7.9927	7.9837	7.9475	8.0090	8.0245	8.0169	7.9862	8.0043
Mg#	63.86	64.56	65.37	67.56	64.86	64.17	68.77	70.35

Contrib Mineral Petrol (2007) 154:371–383
DOI 10.1007/s00410-007-0198-4

eTable 2: Clinopyroxene compositions from the Gb108 runs.

	D-306	C-1856	C-1864	C-1844	C-1860	C-1907	C-1908	C-1910	C-1913
SiO_2	51.64	51.68	51.61	50.95	51.18	51.85	53.03	52.94	51.73
TiO_2	0.43	0.41	0.42	0.35	0.29	0.39	0.39	0.37	0.25
Al_2O_3	16.91	17.50	17.40	16.68	16.32	17.19	17.20	17.02	17.12
Cr_2O_3	0.01	0.01	0.01	0.02	0.02	0.02	0.02	0.01	0.02
FeO	4.62	5.37	5.75	5.44	5.23	4.95	5.30	4.94	4.95
MgO	8.84	9.26	9.43	10.31	11.04	8.94	9.02	9.17	9.87
MnO	0.09	0.12	0.14	0.12	0.13	0.11	0.12	0.12	0.11
NiO	0.01	0.01	0.02	0.01	0.01	0.01	0.02	0.02	0.00
CaO	13.95	13.24	13.09	13.89	14.09	13.16	12.80	13.15	13.16
Na_2O	3.94	3.63	3.31	3.02	3.00	3.37	3.31	3.70	3.47
K_2O	0.01	0.01	0.01	0.01	0.00	0.01	0.01	0.01	0.00
Total	100.45	101.24	101.20	100.79	101.32	100.00	101.21	101.44	100.69
(6 O)									
Si	1.8253	1.8129	1.8122	1.8006	1.7995	1.8336	1.8498	1.8453	1.8198
Ti	0.0115	0.0107	0.0112	0.0092	0.0076	0.0105	0.0102	0.0096	0.0067
Al	0.7049	0.7236	0.7202	0.6950	0.6766	0.7170	0.7075	0.6996	0.7099
Cr	0.0003	0.0004	0.0004	0.0005	0.0004	0.0006	0.0005	0.0002	0.0006
Fe	0.1366	0.1575	0.1689	0.1607	0.1538	0.1463	0.1547	0.1441	0.1456
Mg	0.4656	0.4842	0.4933	0.5428	0.5788	0.4711	0.4690	0.4762	0.5177
Mn	0.0026	0.0034	0.0041	0.0037	0.0039	0.0033	0.0034	0.0037	0.0033
Ni	0.0003	0.0004	0.0006	0.0003	0.0004	0.0004	0.0004	0.0004	0.0001
Ca	0.5282	0.4977	0.4926	0.5261	0.5310	0.4988	0.4785	0.4913	0.4960
Na	0.2703	0.2466	0.2253	0.2071	0.2043	0.2309	0.2236	0.2497	0.2370
K	0.0002	0.0003	0.0004	0.0003	0.0001	0.0005	0.0003	0.0004	0.0001
Total	3.9459	3.9378	3.9292	3.9462	3.9565	3.9129	3.8980	3.9203	3.9368
Mg#	77.31	75.47	74.49	77.16	79.00	76.31	75.17	76.76	78.04
Al-buffonite	0.023	0.021	0.022	0.018	0.015	0.021	0.020	0.019	0.013
Jadeite	0.270	0.247	0.225	0.207	0.204	0.231	0.224	0.250	0.237
Ca-eskolaite	0.108	0.124	0.142	0.108	0.087	0.174	0.204	0.159	0.126
Ca-Tschermak	0.023	0.040	0.032	0.021	0.022	0.012	0.002	0.015	0.037
Diopside	0.428	0.374	0.368	0.432	0.451	0.379	0.354	0.378	0.382
Enstatite	0.026	0.100	0.115	0.101	0.121	0.081	0.105	0.089	0.129
Ferrosilite	0.137	0.157	0.169	0.161	0.154	0.146	0.155	0.144	0.146

Contrib Mineral Petrol (2007) 154:371–383
DOI 10.1007/s00410-007-0198-4

eTable 3: Estimated partial melt compositions from the Gb108 runs. These compositions were obtained by EDS electron microscopy. See text for more details.

	C-1844	C-1860	C-1908	C-1910	C-1913
SiO_2	61.92	57.69	64.36	61.26	56.59
TiO_2	0.65	0.70	1.48	1.17	0.93
Al_2O_3	17.70	18.19	15.35	15.69	16.44
Cr_2O_3					
FeO	5.04	6.03	5.55	6.44	7.01
MgO	2.83	3.61	1.64	2.52	4.49
MnO		0.08	0.09	0.14	0.13
NiO					
CaO	7.02	7.85	7.71	8.45	9.57
Na_2O	4.05	3.40	2.38	2.37	2.60
K_2O	0.19	0.14	0.75	0.36	0.16
Total	99.40	97.68	99.30	98.39	97.90
Mg#	50.00	51.61	34.45	41.09	53.28

Contrib Mineral Petrol (2007) 154:371–383
DOI 10.1007/s00410-007-0198-4

eTable 4: Trace element compositions (ppm) of phases and quenched liquid in Gb108, as determined by SIMS. Abbreviations are as in Table 3.

	C-1907 ga	C-1907 cpx	C-1910 ga	C-1910 cpx	C-1910 L	C-1913 ga	C-1913 cpx	C-1913 L	C-1879 cpx	C-1879 L	C-1891 cpx	C-1891 L
Ba	0.12	2.96	0.72	0.47	14.31			10.20	0.32	6.96	0.51	5.09
Th									0.00	0.02	0.00	0.03
Nb	0.03	0.09	0.03		0.51			0.31	0.02	0.19	0.02	0.19
K	21.3	449	104	85	1686	2.63		1364	60	1009	90.0	699
La	0.01	0.55	0.09	0.17	1.89	0.01	0.06	1.87	0.09	1.40	0.15	1.09
Ce	0.40	1.95	0.31	0.66	6.83	0.08	0.17	6.34	0.42	4.44	0.53	3.47
Pr	0.11	0.38	0.06	0.21	1.16	0.04	0.09	1.28	0.12	0.99	0.13	0.64
Sr	7.78	200	26.6	101	520	2.00	42.2	558.8	60.4	400	63.9	311
Nd	1.35	2.53	0.91	1.22	7.80	0.51	0.38	8.60	0.93	5.88	0.90	4.51
Sm	1.56	0.89	0.95	0.46	1.81	0.63	0.34	2.54	0.41	1.64	0.46	1.62
Zr	36.6	12.3	19.1	5.92	36.8	15.6	2.05	41.4	4.69	31.1	4.41	23.7
Eu	1.41	0.55	0.88	0.43	1.67	0.68	0.17	1.71	0.28	1.33	0.30	0.94
Ti	2438	2723	1926	1901	4732	2183	1434	5482	1790	3477	1503	3787
Gd	5.50	1.19	3.45	1.38	4.28	3.20	0.28	3.78	0.82	2.62	0.70	2.51
Tb	1.09	0.18	0.83	0.30	0.74	0.90	0.07	0.65	0.13	0.43	0.15	0.49
Dy	10.2	1.07	7.12	0.96	4.85	8.51	0.93	4.27	1.14	3.17	1.13	2.56
Y	63.4	5.86	53.2	4.51	23.9	63.9	5.19	19.4	7.26	17.6	6.49	16.0
Ho	1.64	0.17	1.78	0.19	0.92	2.16	0.22	0.62	0.23	0.53	0.19	0.58
Er	7.32	0.59	5.61	0.32	3.26	8.38	0.58	1.94	0.73	1.71	0.63	1.63
Yb	9.19	0.46	7.53	0.46	2.96	12.12	0.42	1.46	0.68	1.66	0.73	1.78